Dancing in the void: hydrodynamical N-body simulations of the extremely metal poor galaxy DDO 68

R. Pascale[1⋆], F. Annibali[1], M. Tosi[1], F. Marinacci[2], C. Nipoti[1,2], M. Bellazzini[1], D. Romano[1], E. Sacchi[3], A. Aloisi[4], M. Cignoni[5,6,7]

[1] *INAF - Osservatorio di Astrofisica e Scienza dello Spazio di Bologna, Via Gobetti 93/3, 40129 Bologna, Italy*
[2] *Dipartimento di Fisica e Astronomia 'Augusto Righi', Università di Bologna, via Gobetti 93/2, 40129, Bologna, Italy*
[3] *Leibniz-Institut für Astrophysik Potsdam, An der Sternwarte 16, 14482 Potsdam, Germany*
[4] *Space Telescope Science Institute, 3700 San Martin Drive, Baltimore, MD 21218, USA*
[5] *Dipartimento di Fisica, Università di Pisa, Largo Bruno Pontecorvo 3, 56127, Pisa, Italy*
[6] *INFN, Largo B. Pontecorvo 3, 56127, Pisa, Italy*
[7] *Osservatorio astronomico di Capodimonte, Vicolo Moiariello 16, 80131, Napoli, Italy*

ABSTRACT

Using hydrodynamical N-body simulations, we show that the observed structure and kinematics of the extremely metal-poor, dwarf irregular galaxy DDO 68 is compatible with a merger event with at least two smaller satellite galaxies. We were able to obtain a self-consistent model that simultaneously reproduces several of its observed features, including: the very asymmetric and disturbed shape of the stellar component, the overall HI distribution and its velocity field, the arc-like stellar structure to the west, the low-surface brightness stellar stream to the north. The model implies the interaction of the main progenitor of DDO 68 with two systems with dynamical masses $7 \times 10^8\ M_\odot$ and almost $10^8\ M_\odot$ – 1/20 and 1/150 times the dynamical mass of DDO 68, respectively. We show that the merger between DDO 68 and the most massive of its satellites offers a route to explain the large offset of DDO 68 from the mass-metallicity relation. Assuming that the interacting galaxies have metallicities prior to the merger compatible with those of galaxies with similar stellar masses, we provide quantitative evidence that gas mixing alone does not suffice at diluting the gas of the two components; according to our simulations, the HII regions observed along the Cometary Tail trace the low metallicity of the accreted satellite rather than that of DDO 68's main body. In this case, the mass corresponding to the low metallicity is that of the secondary body and DDO 68 becomes consistent with the mass-metallicity relation.

12 + log(O/H) = 7.14 ± 0.07

D = 12.65Mpc

Lynx-Cancer void

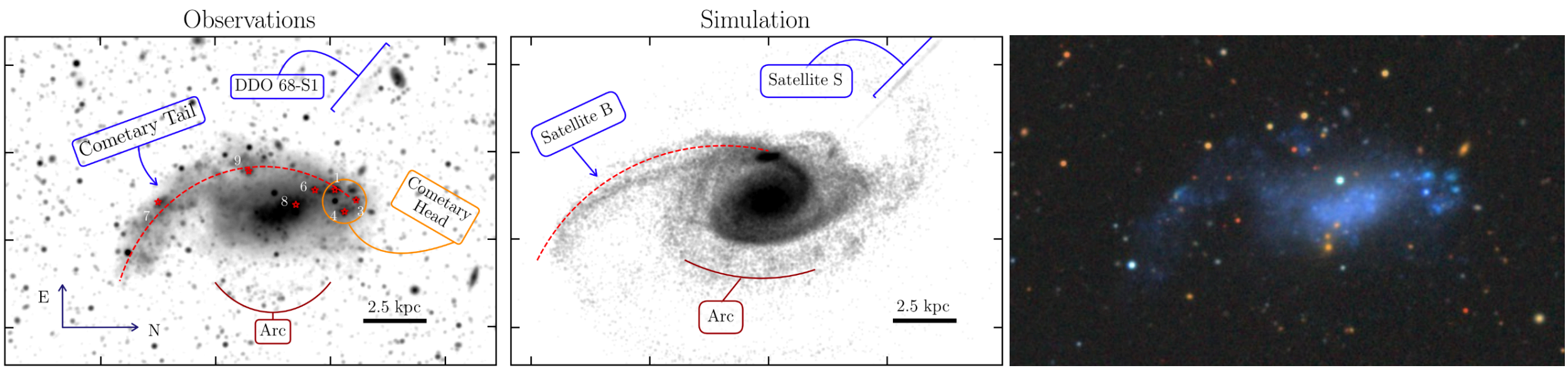

Figure 1. Left panel: LBT g-band image of DDO 68. We show the position of the Cometary Tail (blue arrow), the Cometary Head (yellow circle), where some of the HII regions are clearly visible as dark spots (see text for details), the position of the stellar stream DDO 68-S1 (blue bracket) and the Arc (dark red arc). All the HII regions referred in Fig. 6 are shown by red stars. East is up, North is to the right. Right panel: mock observation of DDO 68 from the simulation of Section 4. All the features reproduced by the simulation are marked as in the left panel (see Section 4 for details on similarities and differences between model and data). Both images have the same surface brightness limit (29 mag arcsec^2), the same spatial resolution (pixel size 0.225 arcsec $\times$ 0.225 arcsec) and the same Gaussian smoothing (FWHM $\simeq$ 1.9 arcsec). In both panels, we follow DDO 68 B from the Tail to the Head with a dashed red line. The field in each panel is $13.8 \times 20.7\,\mathrm{kpc}^2$.

Table 1. Main input parameters used to generate the ICs of the simulations. Galaxy: reference galaxy (DDO 68, Satellite B or Satellite S); $M_{\rm dm}$: total dark matter mass (equation 1); a: dark matter scale radius (equation 1); $M_\star$: total stellar mass (equation 2); $h_\star$ and $z_\star$: stellar disc scale length and scale height, respectively (equation 2); $M_{\rm gas}$: gaseous disc total mass (equation 3); $h_{\rm gas}$: gaseous disc scale length (equation 3).

Galaxy	$M_{\rm dm}$ [$M_\odot$]	a [kpc]	$M_\star$ [$M_\odot$]	$h_\star$ [kpc]	$z_\star$ [kpc]	$M_{\rm gas}$ [$M_\odot$]	$h_{\rm gas}$ [kpc]
DDO 68	1.3×10^{10}	4	1.17×10^8	1.02	0.153	9.4×10^8	5.28
Satellite B	6.5×10^8	1.86	1.2×10^7	0.47	0.0705	0.6×10^8	1.41
Satellite S	8.6×10^7	1.2	3.6×10^6	0.3	0.045	-	-

Код AREPO

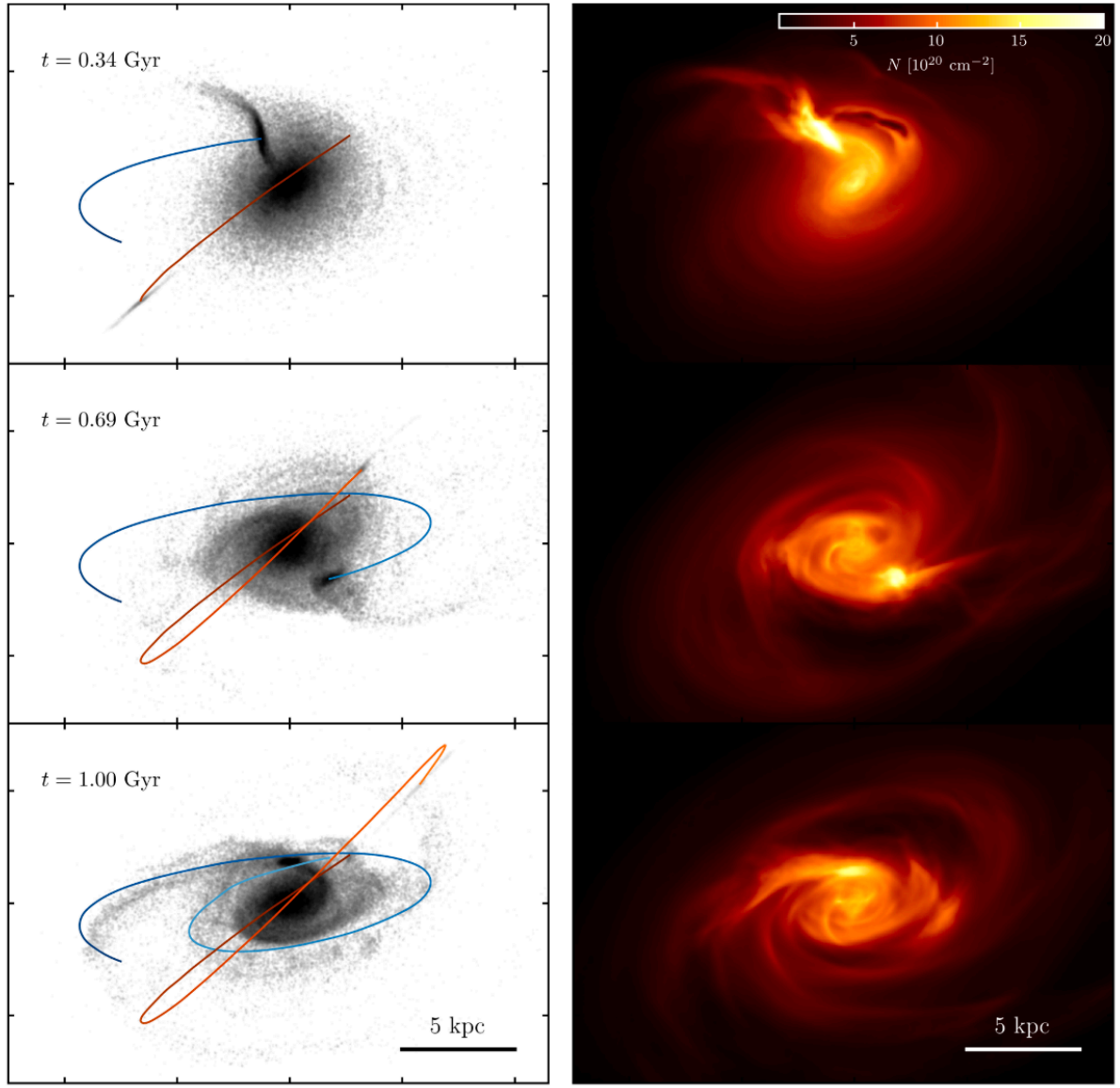

Figure 4. Left panels: stellar surface brightness maps from subsequent snapshots of the reference simulation of Section 4. In each panel the line-of-sight is given by $(\alpha, \gamma, \beta) = (30°, 225°, -20°)$, the pixel size is $0.225\,\mathrm{arcsec} \times 0.225\,\mathrm{arcsec}$, and the maps have been smoothed with a gaussian beam of FWHM $1.9\,\mathrm{arcsec}$, corresponding to a $0.7\,\mathrm{arcsec}$ seeing. The mass-to-light ratios attributed to the particles of DDO 68, Satellite B and Satellite S are $\Upsilon_g^{\mathrm{A}} = 0.51$, $\Upsilon_g^{\mathrm{B}} = 0.51$ and $\Upsilon_g^{\mathrm{S1}} = 5.5$, respectively, and the maps have depth of $29\,\mathrm{mag\,arcsec^{-2}}$. The field in each panel is $18 \times 24\,\mathrm{kpc}^2$ and the sequence of panels (from top to bottom) evolves showing snapshots corresponding to $t = 0.34\,\mathrm{Gyr}$, $t = 0.69\,\mathrm{Gyr}$ and $t = 1\,\mathrm{Gyr}$. The blue and orange lines show the orbits of the centres of mass of the dark matter haloes of Satellite B and Satellite S, respectively, computed with the shrinking sphere method (Power et al. 2003). The bottom left panel shows the same configuration as in the right panel of Fig. 1. Right panels: same as the left panels, but showing the gas projected number density. In this case, the pixel size is $0.68\,\mathrm{arcsec} \times 0.68\,\mathrm{arcsec}$ and the maps are convolved with a $1.9\,\mathrm{arcsec}$ beam. Details on the ICs are given in Section 2.3, and Tables 1 and 3.

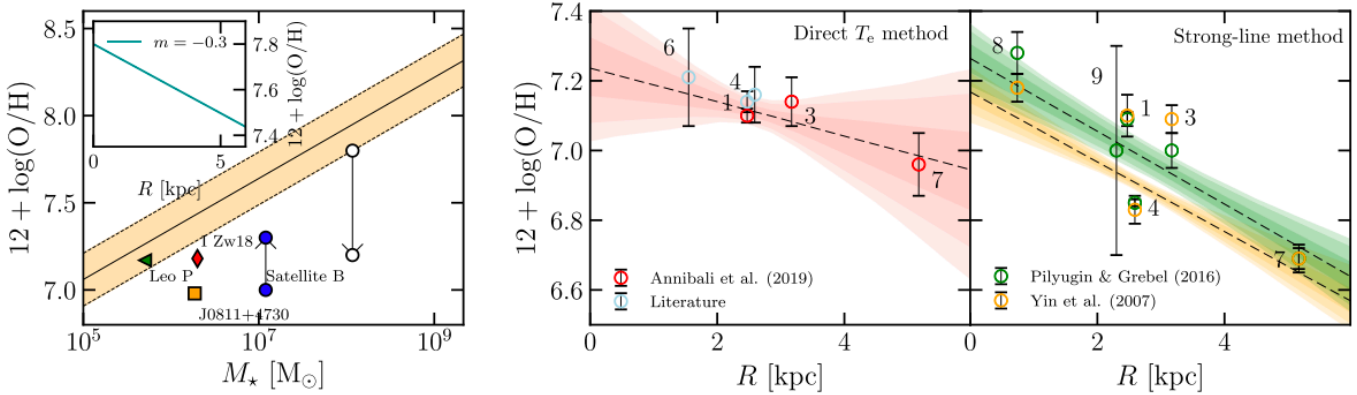

Figure 6. Left panel: MZR relation from Berg et al. (2012). The light orange band shows the intrinsic scatter of the relation while the arrow between the white points starts from the metallicity of DDO 68 in the ICs of the simulation of Section 5 and points at the average measured value. The black arrow between the blue circles starts from the initial oxygen abundance assumed for Satellite B in the simulation and points at the diluted metallicity. The green triangle, yellow square and the red diamond show the position in the mass-metallicity plane of Leo P, J0811+4730 and I Zw 18 respectively. The small inset shows the oxygen abundance as a function of the galactocentric distance (equation 8) in the ICs of the simulation. Middle panel: $12 + \log(\mathrm{O/H})$ from six HII regions of DDO 68 measured with the direct-T_e method as a function of the galactocentric distance. The red and cyan dots are measurements from A19, and Izotov & Thuan (2007, 2009), respectively. We fit the measurements with relation 8 and report the fiducial model (black dashed curve) and the $n\sigma$ uncertanties, with $n = 1, 2, 3$ (light red bands). Right panel: same as the middle panel but showing measurements of the six HII regions from A19 calibrated using strong-line relations from Pilyugin & Grebel (2016, green dots) and Yin et al. (2007, yellow dots), alongside the best fit models. The numbers in the middle- and right-hand panels refer to HII regions in DDO 68 according to the nomenclature of A19 (see Fig. 1). Details on the fits are given in Table 4.

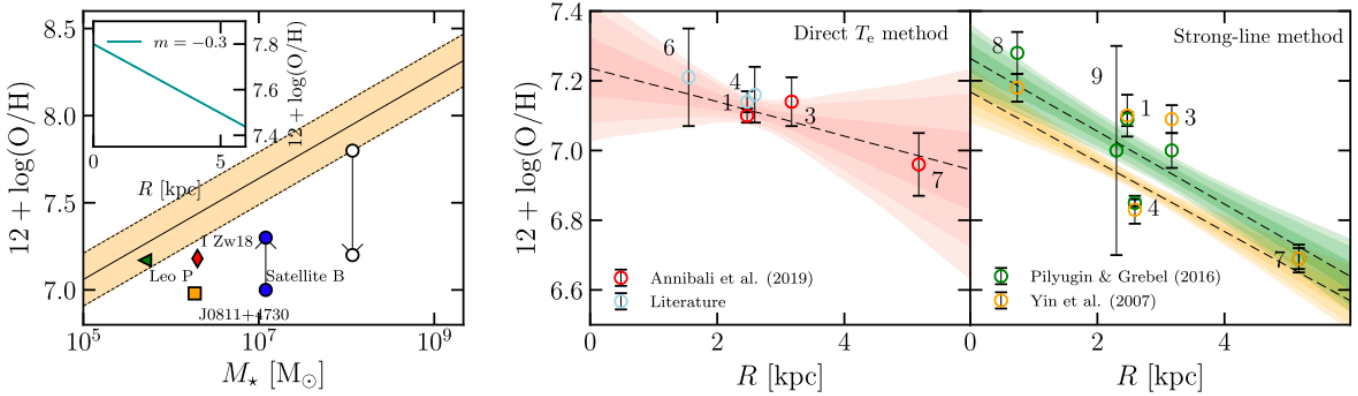

Figure 6. Left panel: MZR relation from Berg et al. (2012). The light orange band shows the intrinsic scatter of the relation while the arrow between the white points starts from the metallicity of DDO 68 in the ICs of the simulation of Section 5 and points at the average measured value. The black arrow between the blue circles starts from the initial oxygen abundance assumed for Satellite B in the simulation and points at the diluted metallicity. The green triangle, yellow square and the red diamond show the position in the mass-metallicity plane of Leo P, J0811+4730 and I Zw 18 respectively. The small inset shows the oxygen abundance as a function of the galactocentric distance (equation 8) in the ICs of the simulation. Middle panel: $12 + \log(\mathrm{O/H})$ from six HII regions of DDO 68 measured with the direct-T_e method as a function of the galactocentric distance. The red and cyan dots are measurements from A19, and Izotov & Thuan (2007, 2009), respectively. We fit the measurements with relation 8 and report the fiducial model (black dashed curve) and the $n\sigma$ uncertanties, with $n = 1, 2, 3$ (light red bands). Right panel: same as the middle panel but showing measurements of the six HII regions from A19 calibrated using strong-line relations from Pilyugin & Grebel (2016, green dots) and Yin et al. (2007, yellow dots), alongside the best fit models. The numbers in the middle- and right-hand panels refer to HII regions in DDO 68 according to the nomenclature of A19 (see Fig. 1). Details on the fits are given in Table 4.

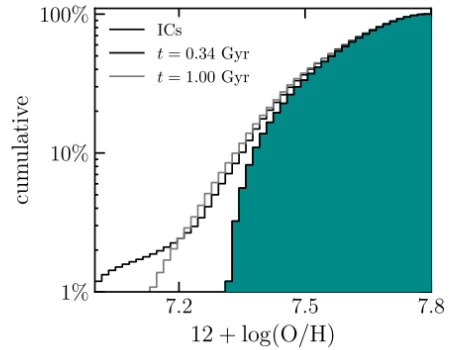

Figure 7. Cumulative, gas-mass weighted metallicity distribution as a function of time for the simulation of Section 5. The curves correspond to distributions computed from the ICs (dark cyan), after $t = 340$ Myr (black curve) and after $t = 1$ Gyr (grey curve).

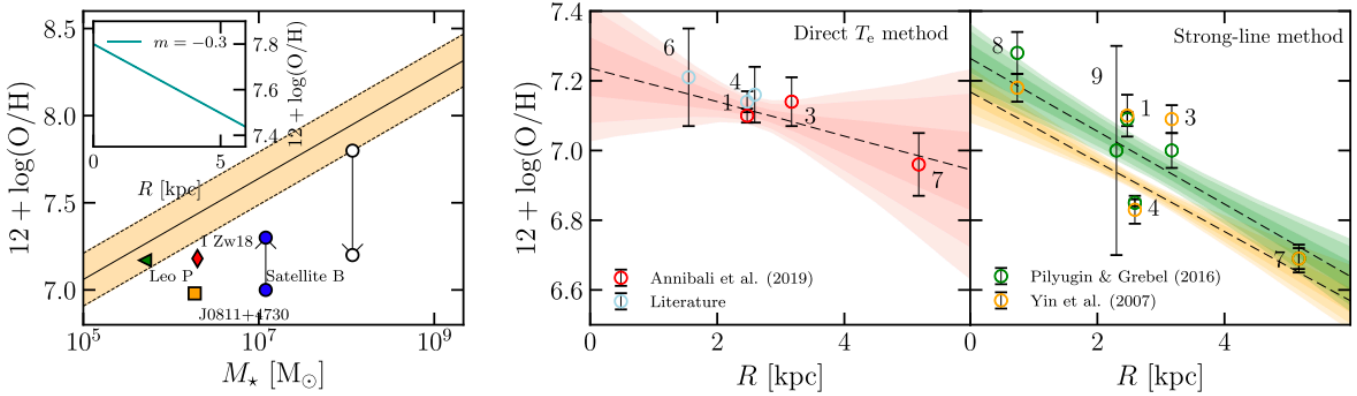

Figure 6. Left panel: MZR relation from Berg et al. (2012). The light orange band shows the intrinsic scatter of the relation while the arrow between the white points starts from the metallicity of DDO 68 in the ICs of the simulation of Section 5 and points at the average measured value. The black arrow between the blue circles starts from the initial oxygen abundance assumed for Satellite B in the simulation and points at the diluted metallicity. The green triangle, yellow square and the red diamond show the position in the mass-metallicity plane of Leo P, J0811+4730 and I Zw 18 respectively. The small inset shows the oxygen abundance as a function of the galactocentric distance (equation 8) in the ICs of the simulation. Middle panel: $12 + \log(\mathrm{O/H})$ from six HII regions of DDO 68 measured with the direct-T_e method as a function of the galactocentric distance. The red and cyan dots are measurements from A19, and Izotov & Thuan (2007, 2009), respectively. We fit the measurements with relation 8 and report the fiducial model (black dashed curve) and the $n\sigma$ uncertanties, with $n = 1, 2, 3$ (light red bands). Right panel: same as the middle panel but showing measurements of the six HII regions from A19 calibrated using strong-line relations from Pilyugin & Grebel (2016, green dots) and Yin et al. (2007, yellow dots), alongside the best fit models. The numbers in the middle- and right-hand panels refer to HII regions in DDO 68 according to the nomenclature of A19 (see Fig. 1). Details on the fits are given in Table 4.

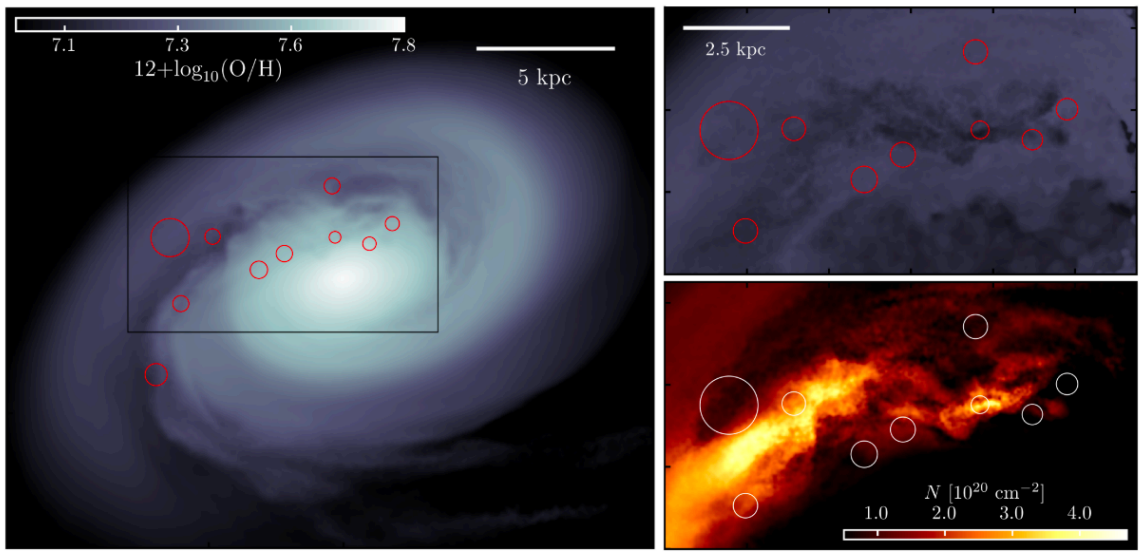

Figure 8. Left panel: gas mass-weighted metallicity map from the simulation of Section 5 with $m = -0.3$. The line-of-sight is the same as in Fig.s 4 and 5 and the simulation has evolved for $t = 1$ Gyr (bottom panels of Fig. 4). Top-right panel: zoom-in view of the region marked with a black box in the left panel. To highlight substructures in the gas of Satellite B, the metallicity map has been obtained considering only gas particles with oxygen abundance $12 + \log(\mathrm{O/H}) < 7.3$ (see right panel of Fig. 7). Bottom-right panel: gas surface density of the weighted metallicity map shown in the top-right panel. The red and white circles in all panels show the regions of extractions used to compute the local oxygen abundances shown in Fig.9.

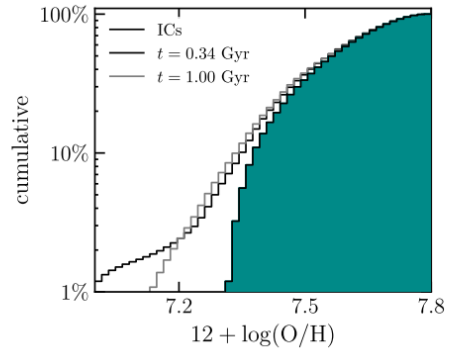

Figure 7. Cumulative, gas-mass weighted metallicity distribution as a function of time for the simulation of Section 5. The curves correspond to distributions computed from the ICs (dark cyan), after $t = 340$ Myr (black curve) and after $t = 1$ Gyr (grey curve).

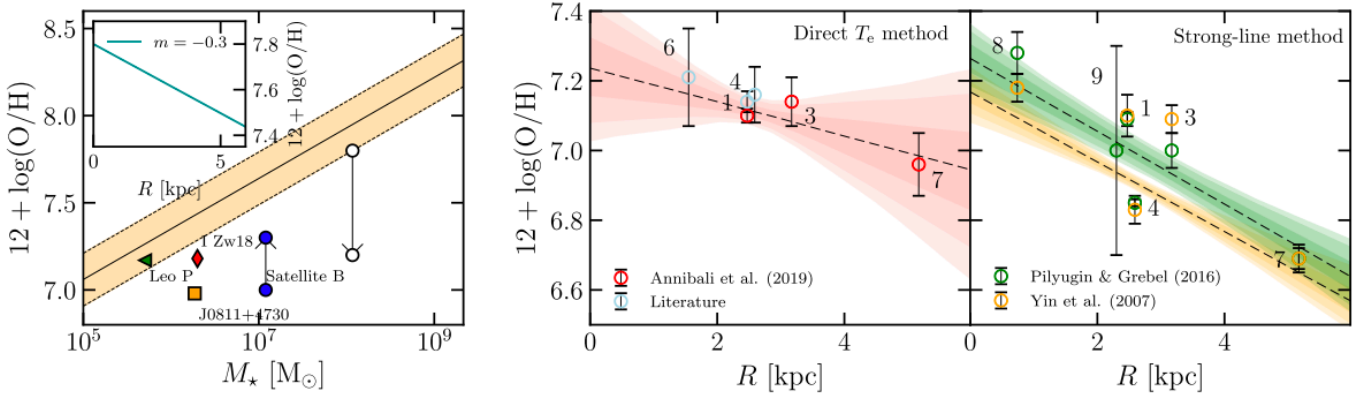

Figure 6. Left panel: MZR relation from Berg et al. (2012). The light orange band shows the intrinsic scatter of the relation while the arrow between the white points starts from the metallicity of DDO 68 in the ICs of the simulation of Section 5 and points at the average measured value. The black arrow between the blue circles starts from the initial oxygen abundance assumed for Satellite B in the simulation and points at the diluted metallicity. The green triangle, yellow square and the red diamond show the position in the mass-metallicity plane of Leo P, J0811+4730 and I Zw 18 respectively. The small inset shows the oxygen abundance as a function of the galactocentric distance (equation 8) in the ICs of the simulation. Middle panel: $12 + \log(O/H)$ from six HII regions of DDO 68 measured with the direct-T_e method as a function of the galactocentric distance. The red and cyan dots are measurements from A19, and Izotov & Thuan (2007, 2009), respectively. We fit the measurements with relation 8 and report the fiducial model (black dashed curve) and the $n\sigma$ uncertanties, with $n = 1, 2, 3$ (light red bands). Right panel: same as the middle panel but showing measurements of the six HII regions from A19 calibrated using strong-line relations from Pilyugin & Grebel (2016, green dots) and Yin et al. (2007, yellow dots), alongside the best fit models. The numbers in the middle- and right-hand panels refer to HII regions in DDO 68 according to the nomenclature of A19 (see Fig. 1). Details on the fits are given in Table 4.

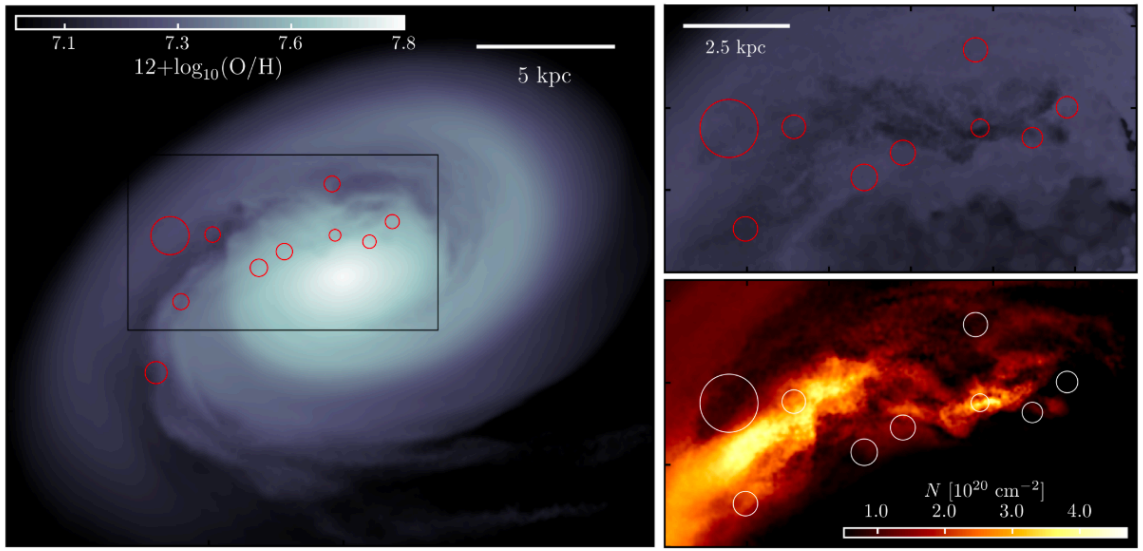

Figure 8. Left panel: gas mass-weighted metallicity map from the simulation of Section 5 with $m = -0.3$. The line-of-sight is the same as in Fig.s 4 and 5 and the simulation has evolved for $t = 1$ Gyr (bottom panels of Fig. 4). Top-right panel: zoom-in view of the region marked with a black box in the left panel. To highlight substructures in the gas of Satellite B, the metallicity map has been obtained considering only gas particles with oxygen abundance $12 + \log(O/H) < 7.3$ (see right panel of Fig. 7). Bottom-right panel: gas surface density of the weighted metallicity map shown in the top-right panel. The red and white circles in all panels show the regions of extractions used to compute the local oxygen abundances shown in Fig.9.

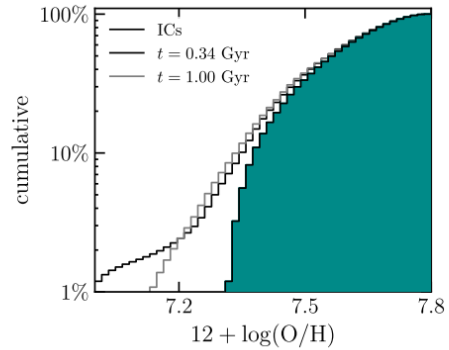

Figure 7. Cumulative, gas-mass weighted metallicity distribution as a function of time for the simulation of Section 5. The curves correspond to distributions computed from the ICs (dark cyan), after $t = 340$ Myr (black curve) and after $t = 1$ Gyr (grey curve).

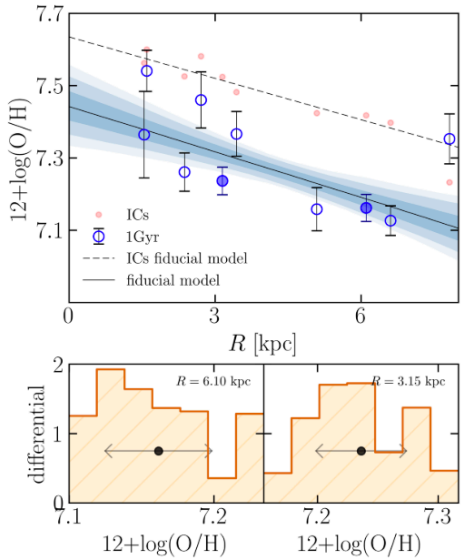

Figure 9. Top panel: oxygen abundance (dots with errorbars) as a function of the projected distance from the centre of the galaxy for the simulation with initial intrinsic metallicity gradient $m = -0.3$, after the simulation has evolved for 1 Gyr. The abundances are computed in the spherical regions along Satellite B, as shown in Fig. 8 (see text for details). The light red dots show the oxygen abundances computed in the same extraction regions but in the ICs. Each measure is plotted as $\mu \pm \sigma$, with μ and σ the mean and dispersion of the gas-mass weighted metallicity distribution of that extraction region, respectively, converted into oxygen abundances. The dashed and solid black lines show the best fit relations 8 derived from the evolved simulation and the ICs (best fit parameters are given in Table 4), respectively. Bottom panels: gas-mass weighted metallicity distribution for two extraction regions marked by full dots in the top panels. The black dots show the mean metallicity while the arrows a region 2σ wide.

Подчеркивают, что их задачей было воспроизвести наблюдаемую картину. Поэтому позволили себе некоторые допущения:

- Относительно низкая начальная металличность DDO68
- Относительно крутой градиент металличности
- Не учитывается ЗО, которое будет обогащать среду металлами

С другой стороны, не исследовали, как будет влиять относительная масса газа в Sat.B (она может быть больше - эффект будет сильнее).

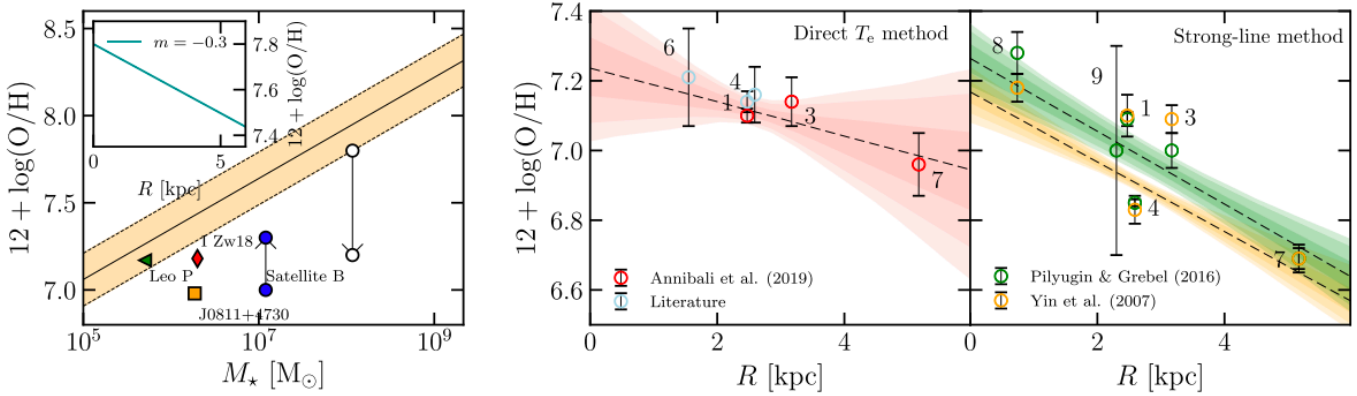

Figure 6. Left panel: MZR relation from Berg et al. (2012). The light orange band shows the intrinsic scatter of the relation while the arrow between the white points starts from the metallicity of DDO 68 in the ICs of the simulation of Section 5 and points at the average measured value. The black arrow between the blue circles starts from the initial oxygen abundance assumed for Satellite B in the simulation and points at the diluted metallicity. The green triangle, yellow square and the red diamond show the position in the mass-metallicity plane of Leo P, J0811+4730 and I Zw 18 respectively. The small inset shows the oxygen abundance as a function of the galactocentric distance (equation 8) in the ICs of the simulation. Middle panel: $12 + \log(\mathrm{O/H})$ from six HII regions of DDO 68 measured with the direct-T_e method as a function of the galactocentric distance. The red and cyan dots are measurements from A19, and Izotov & Thuan (2007, 2009), respectively. We fit the measurements with relation 8 and report the fiducial model (black dashed curve) and the $n\sigma$ uncertanties, with $n = 1, 2, 3$ (light red bands). Right panel: same as the middle panel but showing measurements of the six HII regions from A19 calibrated using strong-line relations from Pilyugin & Grebel (2016, green dots) and Yin et al. (2007, yellow dots), alongside the best fit models. The numbers in the middle- and right-hand panels refer to HII regions in DDO 68 according to the nomenclature of A19 (see Fig. 1). Details on the fits are given in Table 4.

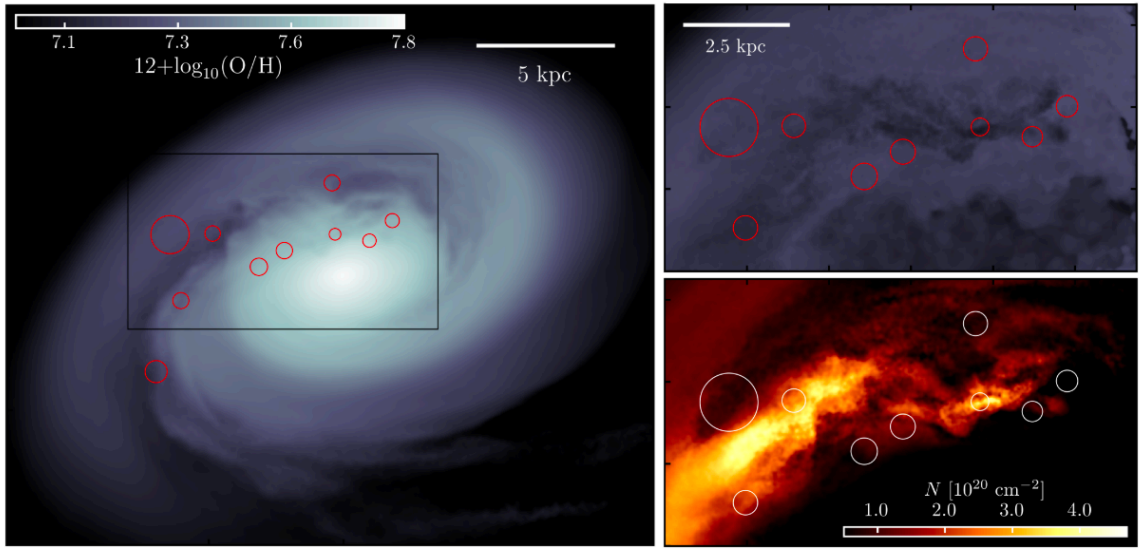

Figure 8. Left panel: gas mass-weighted metallicity map from the simulation of Section 5 with $m = -0.3$. The line-of-sight is the same as in Fig.s 4 and 5 and the simulation has evolved for $t = 1$ Gyr (bottom panels of Fig. 4). Top-right panel: zoom-in view of the region marked with a black box in the left panel. To highlight substructures in the gas of Satellite B, the metallicity map has been obtained considering only gas particles with oxygen abundance $12 + \log(\mathrm{O/H}) < 7.3$ (see right panel of Fig. 7). Bottom-right panel: gas surface density of the weighted metallicity map shown in the top-right panel. The red and white circles in all panels show the regions of extractions used to compute the local oxygen abundances shown in Fig.9.

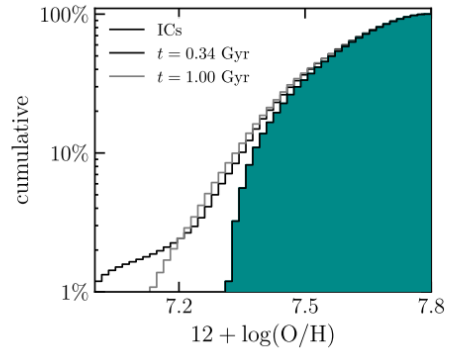

Figure 7. Cumulative, gas-mass weighted metallicity distribution as a function of time for the simulation of Section 5. The curves correspond to distributions computed from the ICs (dark cyan), after $t = 340$ Myr (black curve) and after $t = 1$ Gyr (grey curve).

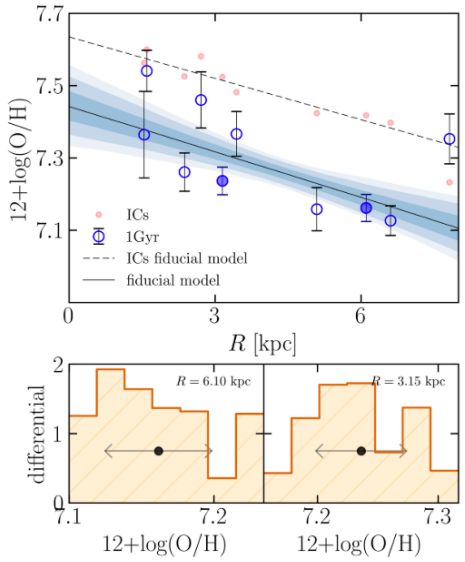

Figure 9. Top panel: oxygen abundance (dots with errorbars) as a function of the projected distance from the centre of the galaxy for the simulation with initial intrinsic metallicity gradient $m = -0.3$, after the simulation has evolved for 1 Gyr. The abundances are computed in the spherical regions along Satellite B, as shown in Fig. 8 (see text for details). The light red dots show the oxygen abundances computed in the same extraction regions but in the ICs. Each measure is plotted as $\mu \pm \sigma$, with μ and σ the mean and dispersion of the gas-mass weighted metallicity distribution of that extraction region, respectively, converted into oxygen abundances. The dashed and solid black lines show the best fit relations 8 derived from the evolved simulation and the ICs (best fit parameters are given in Table 4), respectively. Bottom panels: gas-mass weighted metallicity distribution for two extraction regions marked by full dots in the top panels. The black dots show the mean metallicity while the arrows a region 2σ wide.

Подчеркивают, что их задачей было воспроизвести наблюдаемую картину. Поэтому позволили себе некоторые допущения:

- Относительно низкая начальная металличность DDO68
- Относительно крутой градиент металличности
- Не учитывается ЗО, которое будет обогащать среду металлами

С другой стороны, не исследовали, как будет влиять относительная масса газа в Sat.B (она может быть больше - эффект будет сильнее).

Основные выводы:

- Наблюдаемые особенности можно объяснить результатом взаимодействия трех карликовых галактик
- HII-области, которые используются для оценок металличности, расположены вдоль «хвоста» и соответствуют Спутнику В. Принимаемая для DDO68 металличность на самом деле относится не к самой галактике, а к ее спутнику